2021 27th International Conference on Mechatronics and Machine Vision in Practice (M2VIP) | 978-1-6654-3153-8/21/$31.00 ©2021 IEEE | DOI: 10.1109/M2VIP49856.2021.9665032

Shape Memory Polymer-based Stiffness Variable Soft Actuator Via Digital Light Processing-based 3D Printing

Xinfeng Wei, Honggeng Li, Xiangnan He, Zhenqing Li, Haitao Ye, Wenbo Xue, and Qi Ge

***Abstract*— Variable stiffness actuators have the ability to change stiffness while retaining the advantages of soft actuators, it can be used in an environment requiring a large load. There are many materials used in variable stiffness actuators, among which shape memory polymers (SMP) can change from glassy state to rubber state under temperature change, and its modulus can realize large-span change. At the same time, shape memory polymers under the acrylic acid system have good 3D printable characteristics, so it is more suitable as variable stiffness material. Many researchers have used SMP to make variable stiffness actuators. However, the method of making these reports includes multiple steps, which is very time-consuming and requires high equipment. Our team recently reported a variable stiffness actuator based on digital light processing 3D printing technology (DLP), which can be printed using commercial printers or self-built printers. The variable stiffness layer and actuator cavity can be manufactured by DLP printing technology. At the same time, the materials used can be commercially purchased. The scheme of preparing polymer precursors is very friendly to users without chemical background. The method proposed in this study can quickly and conveniently fabricate variable stiffness actuators based on shape memory polymers.**

I. Introduction

Compared with traditional rigid counterparts, soft actuators made of intrinsically soft materials have gained great attentions because of their excellent environmental adaptivity [1, 2] and safe interaction with human [3]. In recent years, soft actuators have been widely applied to various fields including micro-surgical equipment [4], biomedical systems [5], rehabilitation equipment [6], and many others [1-3]. However, due to low stiffness of soft constituent materials, soft actuators are incompetent in tasks requiring high load capacity [7]. To solve this shortcoming of low load capacity without sacrificing the compliance of soft actuators, researchers have made efforts to develop stiffness variable soft actuators which consist of stiffness variable materials, such as shape memory polymers (SMPs) [8-11], electrorheological materials [12, 13], low melting point alloys (LMPAs) [14, 15]. Among them, SMPs are able to switch stiffness from a few MPa to a few GPa during the glass transition, and therefore considered as one of the most promising stiffness variable materials [16]. Moreover, the recent advancement in (meth)acrylate-based SMPs enables direct 3D printing of SMP structures, which offers an efficient manufacturing approach for SMP-based stiffness variable soft actuators [17-19]. Notably, Zhang et al. reported a hybrid multi-material 3D printing approach to fabricate a fast-response, stiffness variable soft actuator [20]. By optimizing the heating circuit and cooling fluidic channels, the actuator was able to complete a "rigid-soft-rigid" cycle within 32 s. However, in this approach, the main parts of the actuator were manufactured by a commercial Polyjet multi-material 3D printer (Stratasys- J750, Eden Prairie, MN, USA) which is not affordable for many research labs. More importantly, the elastomer and SMP used to fabricate the stiffness-variable actuator were commercial ultraviolet (UV) curable polymers with limited mechanical properties.

In this manuscript, we report a general and inexpensive approach to fabricate a high-performance SMP-based stiffness variable actuator. In this approach, both the soft pneumatic actuator (SPA) part and SMP-based stiffness variable part can be directly fabricated via a digital light processing (DLP)-based 3D printer which only takes half an hour to manufacture the required parts. At the same time, the cost of materials used is about one-tenth of the commercial materials, which are relatively cheap and can be afforded by many research groups. More importantly, both the UV curable elastomer and SMP used here are mechanically robust; the chemicals to prepare them are commercially available, and the protocols for preparing these UV curable polymer precursors are friendly to the users without a chemistry background. The proposed approach paves a simple and versatile way to fabricate SMP-based stiffness-variable soft actuators. This manuscript is arranged as follows: Section 2 introduces the structure design and fabrication process; In Section 3, the preparations of high-performance UV curable elastomer and SMP are presented; In Section 4 and Section 5, we characterize the load capacity as well as the heating and cooling efficiency of the stiffness-variable soft actuator. Section 6 concludes this manuscript.

II. Structure Design and Fabrication Process

As shown in Figure 1a, the stiffness-variable actuator is assembled from three separate parts: a SPA body with a fluidic microchannel for cooling, heating circuit, and SMP-based stiffness variable layers. As shown in Figure 1b, we started the fabrication of the SPA body and SMP layers by using a DLP-based 3D printer. In this work, we used a self-built DLP 3D printer mainly consisting of a digital micromirror device (DMD)-based UV projector (DLP LightCrafter PRO6500S, Wintech, China, wavelength: 385nm), and a translational stage

*Research supported by the National Natural Science Foundation of China (No. 12072142), and the support by the Science, Technology and Innovation Commission of Shenzhen Municipality under grant no. ZDSYS20200811143601004.

X. W., H. L., X. H., Z. L., H. Y., W. X. and Q. G. are with the Department of Mechanical and Energy Engineering, Southern University of Science and Technology, Shenzhen 518055, China.

Q. G. is with Guangdong Provincial Key Laboratory of Human-Augmentation and Rehabilitation Robotics in Universities, Southern University of Science and Technology, Shenzhen 518055, China (corresponding author; e-mail: geq@sustech.edu.cn).

Authorized licensed use limited to: Southern University of Science and Technology. Downloaded on January 12,2022 at 12:33:39 UTC from IEEE Xplore. Restrictions apply.

(MTS50/M-Z8, Thorlabs Inc., Newton, NJ, USA) to control the vertical motion of the printing stage. Other commercial DLP-based 3D printers such as Asiga Pico, Envision TEC, or other similar products can also be used to print the SPA body and SMP layers. To achieve faster heating, we chose conductive silver tape with moderate conductivity and deformability. The Joule heat circuit was patterned by laser cutting. As shown in Figure 1c, we assembled the actuator by stacking all the parts in the sequence presented in Figure 1a. We deposited the precursor solution used to print the SMP layer between different parts, and bonded all the parts by UV curing the assembled actuator for no less than 30 minutes in a commercial UV oven (365nm, UVP Crosslinker CL-1000L, Analytik Jena). Figures 1d-f present the snapshots of the printed parts and assembled soft actuator respectively.

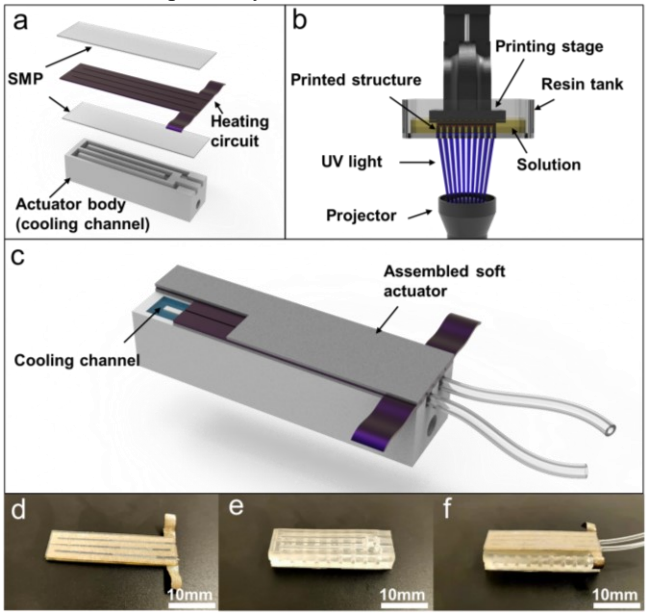

Figure 1. Design and manual fabrication procedures of variable stiffness actuator. (a) Assembly diagram of variable stiffness actuator. (b) Illustration of the DLP-based 3D printing. (c) Schematics of the variable stiffness actuator. (d) Snapshot of the variable stiffness integrated layer. (e) the soft actuator with cooling cavity. (f) An assembled variable stiffness actuator

III. Materials Preparation and Mechanical Properties

A. Stretchable and UV curable Elastomer

Figure 2a shows the chemicals used to prepare highly stretchable and UV curable elastomers, where benzyl acrylate (BA) works as monomer, PEGDA (Mw=700) works as a crosslinker, and 1wt% TPO is added as photo-initiator. All the chemicals were directly purchased from Sigma Aldrich and used as received. Figure 2b presents a schematic illustration of the UV curing process where the monomers and crosslinkers form a covalently boned network. Figure 2c provides the detailed chemical structure of the covalent crosslinking point. Compared with the previously reported butyl acrylate [21] or 2-hydroxyethyl acrylate [22], benzyl acrylate has higher molecular weight, therefor is less odorless and more friendly to laboratory use. As a crosslinker, the content of PEGDA significantly affects the mechanical properties of the polymerization network. Uniaxial tensile tests were carried out to study this effect. The tensile tests were performed on a commercial uniaxial tensile machine (Guangzhou Precision Control Testing Instrument Co. Ltd, XLD-100E, China) and the strain rate was 1.33/min. As shown in Figure 3a, the increase in PEGDA content results in higher Young's Modulus but lower stretchability of the elastomer. As summarized in Figure 3b, the increase in PEGDA content from 0 wt.% to 3 wt.% leads to a slight raise in Young's Modulus from 0.15 MPa to 0.5 MPa but a significant decrease in the elongation-at-break from 3500 % to 500 %. In this work, we prepared the BA-PEGDA elastomer with 1 wt.% of PEGDA whose Young's Modulus is 0.35MPa, and elongation-at-break is 1000 %.

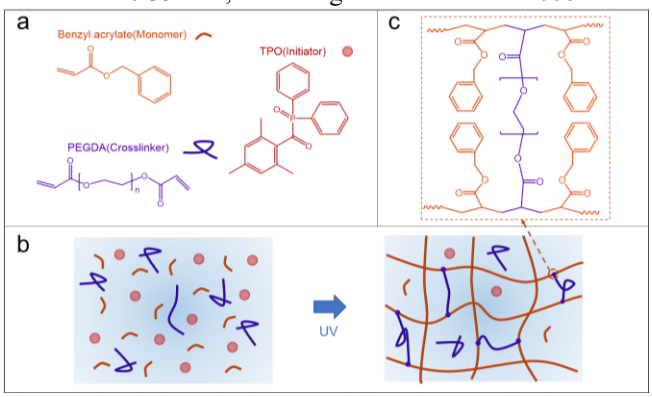

Figure 2. Chemicals used to form stretchable and UV curable Elastomer. (a) Chemicals used to prepare stretchable and UV curable elastomer. (b) Schematic diagram of the polymer network formation process of stretchable and UV-curable elastomers under light. (c) The corresponding chemical structure at crosslinking point of the elastomer.

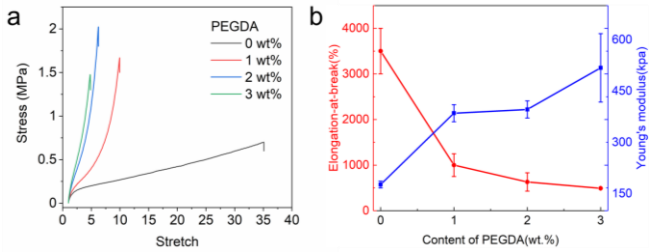

Figure 3. Mechanical property characterization of the stretchable and UV curable Elastomer. (a) Uniaxial tensile tests to investigate the effect of PEGDA content on elastomer's mechanical behavior. (b) Effect of PEGDA content on Young's modulus and elongation-at-break of the BA-PEGDA elastomer.

B. UV curable Shape Memory Polymer

Figure 4a shows the chemicals used to prepare UV curable shape memory polymer where tert-butyl acrylate (*t*BA) works as a monomer in the polymer network, aliphatic urethane diacrylate (AUD) is used as a crosslinker, and 2wt% TPO is added as a photo-initiator. *t*BA and TPO were purchased from Sigma-Aldrich and used without further purification. AUD (Ebecryl 8413) was kindly provided by Allnex. Here, the weight mixing ratio between *t*BA and AUD is 8:2. Figure 4b is the schematic illustration describing the process of forming a photopolymerized network through UV curing. Figure 4c presents the detailed chemical structure at the crosslinking point. It should be noted that the crosslinker AUD imparts high stretchability to the SMP due to its high-molecular weight and the presence of hydrogen bonds between C=O and N-H groups [23]. To study the thermomechanical behavior of *t*BA-AUD SMP, we carried out dynamic mechanical analysis (DMA) tests on a dynamic analyzer (DMA850, TA Instrument Inc., New Castle, DE, USA) by heating from 30 °C to

Authorized licensed use limited to: Southern University of Science and Technology. Downloaded on January 12,2022 at 12:33:39 UTC from IEEE Xplore. Restrictions apply.

70 ℃ at a heating rate of 0.5 ℃/min. As shown in Figure 5a, the glass transition temperature (T_g) of the *t*BA-AUD SMP is identified 57 ℃ through the peak value of tanδ (ratio of loss modulus to storage modulus). It can be seen that when the SMP material changes from glassy state to rubber state, the storage modulus (corresponding to elastic response) decreases from 550MPa at 30 ℃ to 1MPa at 70 ℃, which has a large span modulus decrease and can realize variable stiffness capability. In order to pursue higher variable stiffness efficiency while ensuring the variable stiffness capability of the actuator, the temperature near T_g is selected as the driving temperature. We also used a mechanical testing machine (MTS) (Eden Prairie, MN, USA) to carry out uniaxial tensile tests on SMP materials at different temperatures. The tensile strain rate is 0.67/min. As shown in Figure 5b, the SMP material has a Young's Modulus of 269MPa at room temperature, and when the temperature reaches 58 ℃, the modulus drops to 2MPa. When the actuator is at 58℃, the modulus of the variable stiffness layer is lower and has the ability to deform. Therefore, the driving temperature of the variable stiffness actuator is selected to be 58 ℃.

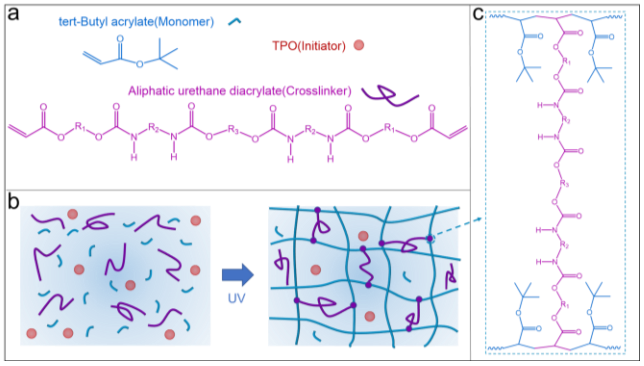

Figure 4. Chemicals used to form UV curable Shape Memory Polymer. (a) Chemicals used to prepare UV curable shape memory polymer. (b) Schematic diagram of the polymer network formation process of UV curable shape memory polymer under light. (c) The corresponding chemical structure at crosslinking point of the SMP.

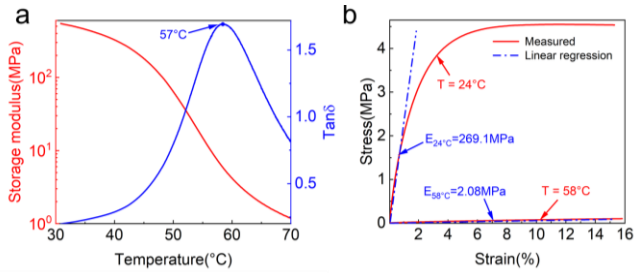

Figure 5. Stiffness-tunable behavior of the SMP material. (a) The DMA characterization of *t*BA-AUD which is chosen as the SMP material. (b) Stress-strain curves of the SMP at 24 and 58 °C.

C. Bonding Characterization between SMP and Elastomer

Since the soft actuator body and SMP layer were bonded through UV curing, it is necessary to measure interfacial toughness between the two constituent materials. Figure 6a presents the schematic illustration of a 180° peeling test where a backing layer was attached to the elastomer to constrain its deformation. The SMP material and the elastomer were bonded in an area of 13 mm × 25 mm. The dimensions of both SMP and elastomer samples are 50 mm × 13 mm × 1 mm (length × width × thickness). The peel test was carried out on a mechanical tensile machine (MTS) (Eden Prairie, MN, USA) at a tensile speed of 10 mm/min. Figure 6b shows the snapshots during the peel test. Figure 6c presents the Force/Width-Displacement relation during the peeling test. The interfacial toughness is about 800N/m indicating that the interfacial bonding between the elastomer and SMP is strong. This strong interfacial bonding can be further confirmed by the inset image of Figure 6c where the elastomer-SMP hybrid samples fractured on the elastomer side rather than at the interface.

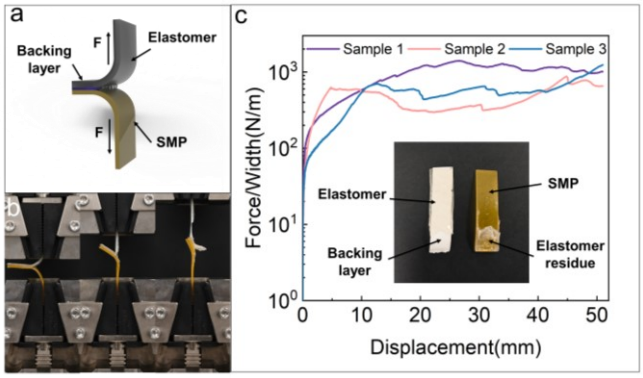

Figure 6. Peeling test to investigate elastomer-SMP bonding interfaces. (a) illustration of 180° peeling test. (b) Snapshot of peel test. (c) The force/width-displacement curves to investigate the interfacial toughness.

IV. Stiffness Variation Characterization.

In order to study the stiffness variation capability of the actuator, we monitor the temperature of the actuator by using a temperature-sensitive resistor. As shown in Figure 7a, the compression fixture of the mechanical testing machine (MTS) and external fixing equipment is used to test the stiffness of actuators in different states. The experimental setup is shown in Figure 7b. We use the heating circuit to heat the actuator to a specified temperature, and then use the experimental device to test the stiffness. The testing device tests the stiffness of the actuator in three states, namely, the actuator at normal temperature (SMP is stiff at this time), the actuator at 58 ℃ (SMP is soft at this time), and the soft actuator without variable stiffness layer. By controlling the test device to drop at a speed of 10mm/min, the force value during the 5mm drop of the compression fixture is recorded. Figure 7c shows the test results of the variable stiffness actuator under different conditions through repeated experiments. The data show that the stiffness of the actuator is 1.71 N/mm at room temperature. When heated to 58 ℃, the stiffness of the actuator is reduced to 0.35 N/mm, and the stiffness of the pure software actuator is 0.25 N/mm. Compared with the actuator in the heated state, the pure software actuator does not drop much, because the SMP layer is only 2mm, which is thinner than the overall size. At the same time, because the structural design of the soft actuator is an integral coated structure, the soft body has greater rigidity. Therefore, when the SMP layer is removed, the rigidity changes little. In figure 7d, we compare the stiffness of variable stiffness actuators made of SMP materials in recent years. The stiffness of our actuators is much higher than that of other actuators.

Authorized licensed use limited to: Southern University of Science and Technology. Downloaded on January 12,2022 at 12:33:39 UTC from IEEE Xplore. Restrictions apply.

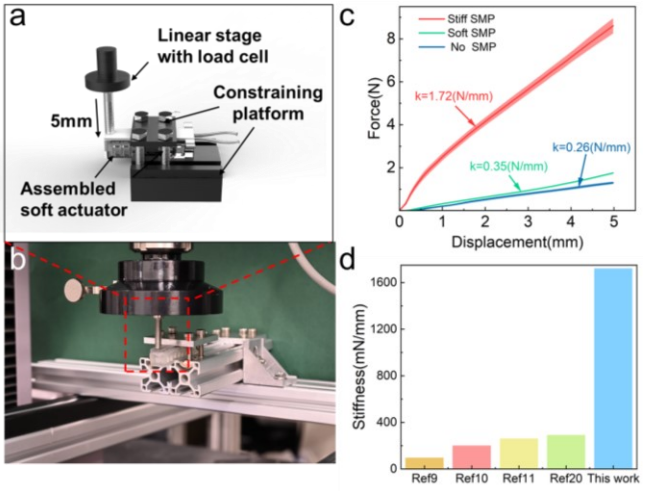

Figure 7. Variable stiffness ability test of variable stiffness actuator. (a) Schematic diagram of actuator stiffness test. (b) Snapshot of actuator stiffness test. (c) The force-displacement curves to investigate variable stiffness ability. (d) Comparison of stiffness with relevant works in the literature.

V. Characterization on Heating and Cooling Efficiencies

To achieve faster heating efficiency, we cut the conductive silver-tape by using a laser cutting machine. From the formula heating power $P=I^2R$, where I is the current and R is the resistance of heating circuit. It can be seen that under the same current, the higher the power R, the greater the power. At the same time, the resistance formula is $R=\rho\times l\times A^{-1}$, where ρ is the resistivity, l is the length, and A is the cross-sectional area. By cutting the conductive tape, the resistance length is increased and the cross-sectional area is reduced, thus increasing the circuit resistance and increasing the generation of Joule heat. To characterize the heating efficiency, we attach a temperature-sensitive resistor to the surface of the actuator to measure the real-time temperature. Figure 8a is a schematic diagram of a temperature test. Figure 8b is an experimental diagram of a temperature test. The heating power supply is 10 V with a current of 1.7 A, and water at 25 ℃ at room temperature is used for cooling. Figure 8c is the acquired temperature-time curve. The driving temperature of SMP material is set at 58 ℃, so the temperature curve only selects the specified temperature range for research. It can be seen that it takes 8 s to rise from normal temperature to driving temperature and 32 s to cool down. To compare heating and cooling efficiencies, we correspond to other variable stiffness actuators in the reference. Figure 8d shows the comparison of heating and cooling efficiencies of different variable stiffness actuators in recent years. It can be seen from the comparison result that the actuators we made is better than some actuators in variable stiffness efficiency. The cooling effect in this study is poor due to the higher temperature of the cooling water, low-temperature cooling water (4 ℃) was used in the high-efficiency cooling experiment [20]. In order to observe the diffusion of the actuator after heating, we used infrared cameras (R550, NEC AVIO, Japan) to photograph the heating process. As shown in Figure 8e, it can be seen that the diffusion is relatively uniform, and the uneven part may be due to uneven heat transfer caused by local material used for bonding differences.

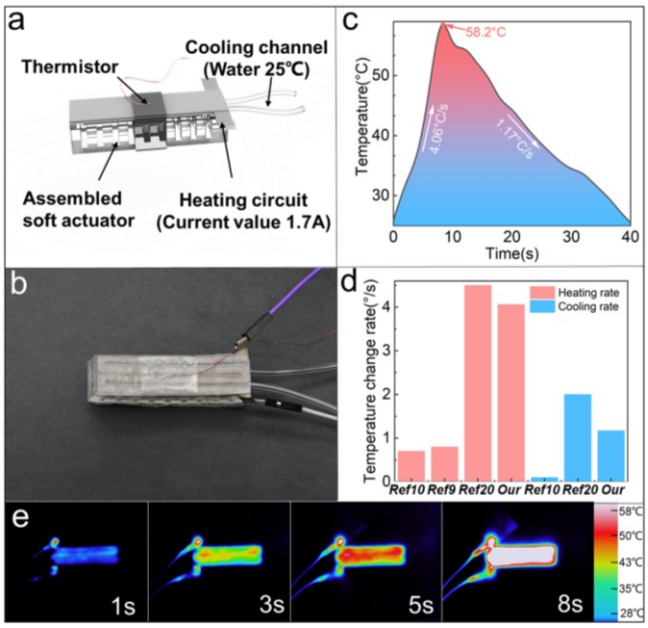

Figure 8. Characterization on Heating and Cooling Efficiencies. (a) Schematic diagram of temperature measuring device (b) Snapshot of temperature test. (c) The temperature-time curves to investigate heating and cooling efficiencies. (d) Comparison of temperature change rate with relevant works in the literature. (e) Real-time heat transfer images taken by infrared cameras.

VI. Conclusion and Future Works

In this work, using commercially available chemical materials to prepare the precursor of photocurable material by a simple process and using the digital light processing 3D printing technology, an actuator with variable stiffness characteristics can be conveniently and quickly manufactured. The printer can be built by itself or a commercial DLP printer can be used. The preparation process is suitable for the design of variable stiffness actuators for most research teams. Since the overall stiffness of the variable stiffness actuator is provided by the soft actuator and the variable stiffness layer together. In this study, because the soft actuator uses a completely encased body, the structure itself already has a larger structure stiffness. The lower limit of the variable stiffness range is higher. In order to pursue a variable stiffness rate at a certain speed, the variable stiffness layer used is thinner, that is, the upper limit of the variable stiffness range is lower. Due to the above two reasons, the overall variable stiffness range is small. The structure will be optimized later to increase the variable stiffness range while ensuring the variable stiffness efficiency. At the same time, conductive tape with good conductivity and ductility is used for heating, and the heating efficiency is significantly improved, but the cooling efficiency needs to be further improved. The current cooling channels are distributed in the lower part of the variable stiffness layer, and cannot achieve rapid cooling during temperature conduction. The cavity will be complicated by 3D printing in the future so that the cavities can wrap the variable stiffness layer to a greater extent to achieve faster cooling.

References

1. Shepherd, R.F., et al., *Soft Machines That are Resistant to Puncture and That Self Seal.* Advanced Materials, 2013. **25**(46): p. 6709-6713.

Authorized licensed use limited to: Southern University of Science and Technology. Downloaded on January 12,2022 at 12:33:39 UTC from IEEE Xplore. Restrictions apply.

2. Deimel, R. and O. Brock, *A novel type of compliant and underactuated robotic hand for dexterous grasping.* International Journal of Robotics Research, 2016. **35**(1-3): p. 161-185.
3. Wehner, M., et al., *An integrated design and fabrication strategy for entirely soft, autonomous robots.* Nature, 2016. **536**(7617): p. 451-+.
4. Ranzani, T., et al., *A bioinspired soft manipulator for minimally invasive surgery.* Bioinspiration & Biomimetics, 2015. **10**(3).
5. Goudu, S.R., et al., *Biodegradable Untethered Magnetic Hydrogel Milli-Grippers.* Advanced Functional Materials, 2020. **30**(50).
6. Polygerinos, P., et al., *Soft robotic glove for combined assistance and at-home rehabilitation.* Robotics and Autonomous Systems, 2015. **73**: p. 135-143.
7. Manti, M., V. Cacucciolo, and M. Cianchetti, *Stiffening in Soft Robotics A Review of the State of the Art.* Ieee Robotics & Automation Magazine, 2016. **23**(3): p. 93-106.
8. Takashima, K., et al., *Pneumatic artificial rubber muscle using shape-memory polymer sheet with embedded electrical heating wire.* Smart Materials and Structures, 2014. **23**(12).
9. Yang, Y., et al., *Novel Design and Three-Dimensional Printing of Variable Stiffness Robotic Grippers.* Journal of Mechanisms and Robotics-Transactions of the Asme, 2016. **8**(6).
10. Yang, Y., et al., *Bioinspired Robotic Fingers Based on Pneumatic Actuator and 3D Printing of Smart Material.* Soft Robot, 2017. **4**(2): p. 147-162.
11. Yang, Y., et al., *Novel Variable-Stiffness Robotic Fingers with Built-In Position Feedback.* Soft Robot, 2017. **4**(4): p. 338-352.
12. Mavroidis, C., *Development of advanced actuators using shape memory alloys and electrorheological fluids.* Research in Nondestructive Evaluation, 2002. **14**(1): p. 1-32.
13. Tonazzini, A., et al., *Variable Stiffness Fiber with Self-Healing Capability.* Advanced Materials, 2016. **28**(46): p. 10142-10148.
14. Shan, W.L., T. Lu, and C. Majidi, *Soft-matter composites with electrically tunable elastic rigidity.* Smart Materials and Structures, 2013. **22**(8).
15. Van Meerbeek, I.M., et al., *Morphing Metal and Elastomer Bicontinuous Foams for Reversible Stiffness, Shape Memory, and Self-Healing Soft Machines.* Advanced Materials, 2016. **28**(14): p. 2801-2806.
16. Xie, T., *Recent advances in polymer shape memory.* Polymer, 2011. **52**(22): p. 4985-5000.
17. Ge, Q., H.J. Qi, and M.L. Dunn, *Active materials by four-dimension printing.* Applied Physics Letters, 2013. **103**(13).
18. Ge, Q., et al., *Active origami by 4D printing.* Smart Materials and Structures, 2014. **23**(9).
19. Ge, Q., et al., *Multimaterial 4D Printing with Tailorable Shape Memory Polymers.* Scientific Reports, 2016. **6**.
20. Zhang, Y.F., et al., *Fast-Response, Stiffness-Tunable Soft Actuator by Hybrid Multimaterial 3D Printing.* Advanced Functional Materials, 2019. **29**(15).
21. Shi, L., et al., *Highly stretchable and transparent ionic conducting elastomers.* Nature Communications, 2018. **9**.
22. Shi, L., et al., *Highly Stretchable and Transparent Ionic Conductor with Novel Hydrophobicity and Extreme-Temperature Tolerance.* Research (Wash D C), 2020. **2020**: p. 2505619.
23. Zhang, B., et al., *Mechanically Robust and UV-Curable Shape-Memory Polymers for Digital Light Processing Based 4D Printing.* Advanced Materials, 2021.

Authorized licensed use limited to: Southern University of Science and Technology. Downloaded on January 12,2022 at 12:33:39 UTC from IEEE Xplore. Restrictions apply.